Physics Letters B 774 (2017) 91–97

Contents lists available at ScienceDirect

Physics Letters B

www.elsevier.com/locate/physletb

Second moment of the pion distribution amplitude with the momentum smearing technique ☆

G.S. Bali [a,b], V.M. Braun [a], M. Göckeler [a], M. Gruber [a], F. Hutzler [a,*], P. Korcyl [a,c], B. Lang [a], A. Schäfer [a]

[a] Institut für Theoretische Physik, Universität Regensburg, 93040 Regensburg, Germany
[b] Department of Theoretical Physics, Tata Institute of Fundamental Research, Homi Bhabha Road, Mumbai 400005, India
[c] Marian Smoluchowski Institute of Physics, Jagiellonian University, ul. Łojasiewicza 11, 30-348 Kraków, Poland

ARTICLE INFO

Article history:
Received 13 June 2017
Received in revised form 16 August 2017
Accepted 28 August 2017
Available online 19 September 2017
Editor: A. Ringwald

Keywords:
Lattice QCD
Pion wave function

ABSTRACT

Using the second moment of the pion distribution amplitude as an example, we investigate whether lattice calculations of matrix elements of local operators involving covariant derivatives may benefit from the recently proposed momentum smearing technique for hadronic interpolators. Comparing the momentum smearing technique to the traditional Wuppertal smearing we find—at equal computational cost—a considerable reduction of the statistical errors. The present investigation was carried out using $N_f = 2 + 1$ dynamical non-perturbatively order a improved Wilson fermions on lattices of different volumes and pion masses down to 220 MeV.

1. Introduction

Many quantities of interest in high-energy physics involve hadrons carrying large momenta. The prime example is provided by form factors, but also parton distribution functions (PDFs) and their generalizations, in particular transverse momentum dependent parton distribution functions (TMDs) receive their physical interpretation in the large-momentum limit.

Very high accuracy is expected for future experimental data, e.g., on hard exclusive and semi-inclusive reactions at the JLAB 12 GeV upgrade [1] and at the Electron Ion Collider (EIC) [2], as well as on B-meson decay and pion transition form factors at Belle II at KEK [3]. This accuracy has to be matched by an increased theoretical precision. Such processes are usually studied using factorization techniques, where the nonperturbative input is reduced to operator matrix elements which, ideally, should be computed using lattice QCD. However, this might require the simulation of hadrons with larger momenta, which increases the statistical noise. Even in the cases where no momentum transfer takes place between the initial and the final state one usually needs to realize hadrons with nonvanishing momenta on the lattice if one wishes to employ operators with sufficiently simple renormalization patterns. It has also been argued [4,5] that hadron sources with large momenta offer novel opportunities, enabling a more direct calculation of parton distributions and hadronic light-cone wave functions by performing a collinear factorization of suitably chosen Euclidean correlation functions (e.g., "quasi-PDFs" [5]), thereby circumventing the traditional Wilsonian local operator product expansion.

Although the problem is known for quite some time, up to very recently [6] no satisfactory techniques for hadrons carrying high momenta on the lattice existed to suppress excited state contributions while maintaining acceptable signal-to-noise ratios. The generic method of reducing excited state overlaps consists of employing carefully tuned extended interpolators. However, for larger momenta the usual smearing techniques become increasingly less effective. The basic idea of Ref. [6] was to modify the usual quark smearing functions by additional phase factors such that the centre of the distribution in momentum space is shifted towards the desired value. By implication, such smearing functions correspond to oscillating wave packets in position space.

It was shown that this technique, which we will refer to as momentum smearing, leads to considerably improved signal-to-noise ratios for the pion and the nucleon two-point functions [6] as well as for lattice observables that are related to quasi-PDFs [7]. In this letter we address another class of applications, namely computing hadronic matrix elements that contain local operators with covariant derivatives, e.g., moments of parton distributions and distribution amplitudes (DAs) [8–13]. In the case that we specifically

☆ RQCD Collaboration.

* Corresponding author.
E-mail address: fabian.hutzler@ur.de (F. Hutzler).

http://dx.doi.org/10.1016/j.physletb.2017.08.077

study, i.e., moments of DAs, the matrix elements of interest are proportional to powers of the hadron momentum and are known, empirically, to be very noisy when using traditional methods. We will demonstrate that momentum smearing results in a major improvement of the quality of the signal for the second moment of the pion DA. In fact, it turns out that this technique is so effective that, at small pion masses and large lattice volumes, statistical fluctuations can be further reduced by deliberately selecting a momentum that is larger than the smallest possible choice.

The scope of the present study is mainly methodological. In addition, we present the first lattice calculation of the 2nd moment of the pion DA using $N_f = 2+1$ dynamical clover Wilson fermions. The results are compatible with the latest $N_f = 2$ study [12], while the second moment is somewhat smaller than what has been reported in a simulation employing $N_f = 2+1$ domain wall fermions, which has been carried out at a coarser lattice spacing and at larger quark masses [10].

2. General formalism

2.1. Continuum definitions

Pseudoscalar mesons like the pion have only one independent leading twist (twist two) DA, ϕ, which is defined via a meson-to-vacuum matrix element of renormalized non-local quark–antiquark light-ray operators,

$$\langle 0|\bar{d}(z_2 n)\not{n}[z_2 n, z_1 n]\gamma_5 u(z_1 n)|\pi^+(p)\rangle = \\ = i f_\pi (p\cdot n)\int_0^1 dx\, e^{-i(z_1 x + z_2(1-x))p\cdot n}\phi(x,\mu^2), \tag{1}$$

where $z_{1,2}$ are real numbers, n^μ is an auxiliary light-like vector with $n^2 = 0$, and $|\pi^+(p)\rangle$ represents the ground state pseudoscalar π^+ meson with on-shell momentum $p^2 = m_\pi^2$. The straight path-ordered Wilson line connecting the quark fields, $[z_2 n, z_1 n]$, is inserted to ensure gauge invariance. The scale dependence of ϕ is indicated by the argument μ^2.

Neglecting both isospin breaking and electromagnetic effects, the DAs of the charged pseudoscalar $\pi^\pm$ and the neutral π^0 are trivially related such that it is sufficient to consider only one of them. The decay constant f_π appearing in Eq. (1) can be obtained as the matrix element of a local operator,

$$\langle 0|\bar{d}(0)\gamma_0\gamma_5 u(0)|\pi^+(p)\rangle = i f_\pi p_0, \tag{2}$$

and has a value of $f_\pi \approx 130$ MeV [14].

The physical interpretation of Eq. (1) is that the fraction x of the pion momentum is carried by the u quark, while the $\bar{d}$ antiquark carries the remaining fraction $1-x$. Hence the difference of the momentum fractions,

$$\xi = x - (1-x) = 2x - 1, \tag{3}$$

contains all nontrivial information and its moments are defined as

$$\langle \xi^n \rangle = \int_0^1 dx\,(2x-1)^n \phi(x,\mu^2). \tag{4}$$

Since the Gegenbauer polynomials $C_n^{3/2}(2x-1)$, which correspond to irreducible representations of the collinear conformal group $\mathrm{SL}(2,\mathbb{R})$, form a complete set of functions, the DAs can be expanded as

$$\phi(x,\mu^2) = 6x(1-x)\left[1 + \sum_{n=1}^{\infty} a_n(\mu^2) C_n^{3/2}(2x-1)\right], \tag{5}$$

where the Gegenbauer moments a_n renormalize multiplicatively in leading logarithmic order. Higher-order contributions in the Gegenbauer expansion are suppressed at large scales, since the anomalous dimensions of a_n increase with n. Hence, in the asymptotic limit $\mu \to \infty$ only the leading term survives, which gives:

$$\phi(x, \mu\to\infty) = \phi^{\mathrm{as}}(x) = 6x(1-x). \tag{6}$$

2.2. Lattice definitions

From now on we will work in Euclidean spacetime and follow the conventions of Ref. [12]. The renormalized light-ray operator on the left-hand side of Eq. (1) generates renormalized local operators. This means that Mellin moments of the DAs, see Eq. (4), can be expressed in terms of matrix elements of local operators and can be evaluated using lattice QCD. In order to calculate the second moment of the pion DA ($n = 2$), we define the bare operators

$$\mathcal{P}(x) = \bar{d}(x)\gamma_5 u(x), \tag{7}$$

$$\mathcal{A}_\rho(x) = \bar{d}(x)\gamma_\rho\gamma_5 u(x), \tag{8}$$

$$\mathcal{O}^-_{\rho\mu\nu}(x) = \bar{d}(x)\left[\overleftarrow{D}_{(\mu}\overleftarrow{D}_\nu - 2\overleftarrow{D}_{(\mu}\overrightarrow{D}_\nu + \overrightarrow{D}_{(\mu}\overrightarrow{D}_\nu\right]\gamma_{\rho)}\gamma_5 u(x), \tag{9}$$

$$\mathcal{O}^+_{\rho\mu\nu}(x) = \bar{d}(x)\left[\overleftarrow{D}_{(\mu}\overleftarrow{D}_\nu + 2\overleftarrow{D}_{(\mu}\overrightarrow{D}_\nu + \overrightarrow{D}_{(\mu}\overrightarrow{D}_\nu\right]\gamma_{\rho)}\gamma_5 u(x), \tag{10}$$

where D_μ is the covariant derivative, which will be replaced by a symmetric discretized version on the lattice. In order to obtain a leading twist projection we symmetrize over all Lorentz indices and subtract all traces. This procedure is indicated by enclosing the indices in parentheses, for example $\mathcal{O}_{(\mu\nu)} = \frac{1}{2}\left(\mathcal{O}_{\mu\nu} + \mathcal{O}_{\nu\mu}\right) - \frac{1}{4}\delta_{\mu\nu}\mathcal{O}_{\lambda\lambda}$.

By using the shorthand notation $\overleftrightarrow{D}_\mu = \overrightarrow{D}_\mu - \overleftarrow{D}_\mu$, the operator $\mathcal{O}^-_{\rho\mu\nu}$ can also be written as

$$\mathcal{O}^-_{\rho\mu\nu}(x) = \bar{d}(x)\overleftrightarrow{D}_{(\mu}\overleftrightarrow{D}_\nu\gamma_{\rho)}\gamma_5 u(x). \tag{11}$$

The operator $\mathcal{O}^+_{\rho\mu\nu}$ is, in the continuum, given by the second derivative of the axial-vector current:

$$\mathcal{O}^+_{\rho\mu\nu}(x) = \partial_{(\mu}\partial_\nu \mathcal{A}_{\rho)}(x). \tag{12}$$

This is not the case on the lattice due to discretization effects of the derivatives which can be numerically sizable. The mixing with operators of lower dimension can be prevented by selecting lattice operators that belong to a suitable irreducible representation of the hypercubic group H(4) [9,10]. For our case, this corresponds to choosing all indices different for the operators $\mathcal{O}^\pm$. Identifying one index with the temporal direction, this leaves us with the operators

$$\mathcal{O}^\pm_{4jk}, \quad j,k \in \{1,2,3\},\ j \neq k. \tag{13}$$

In order to extract the desired moments we use two-point correlation functions of the operators $\mathcal{O}^\pm_{4jk}$ and $\mathcal{A}_\rho$ with an interpolating field,

$$C_\rho(t,\boldsymbol{p}) = a^3\sum_{\boldsymbol{x}} e^{-i\boldsymbol{p}\boldsymbol{x}}\langle \mathcal{A}_\rho(\boldsymbol{x},t)\, J^\dagger(0)\rangle, \tag{14}$$

$$C^\pm_{\rho\mu\nu}(t,\boldsymbol{p}) = a^3\sum_{\boldsymbol{x}} e^{-i\boldsymbol{p}\boldsymbol{x}}\langle \mathcal{O}^\pm_{\rho\mu\nu}(\boldsymbol{x},t)\, J^\dagger(0)\rangle, \tag{15}$$

where $J = \mathcal{P}$ or $J = \mathcal{A}_4$. For sufficiently large t, the ground state dominates and the correlation functions give

$$C_{\mathcal{O}}(t,\boldsymbol{p}) = \frac{1}{2E}\langle 0|\mathcal{O}(0)|\pi^+(p)\rangle\langle\pi^+(p)|\, J^\dagger(0)|0\rangle \\ \times\left(e^{-Et} + \tau_{\mathcal{O}}\tau_J e^{-E(T-t)}\right), \tag{16}$$

where the sign factors $\tau_{\mathcal{O}}, \tau_J = \pm 1$ depend on the transformation properties of the correlation functions under time reversal.

Following Ref. [12], the required matrix elements for the second moments can be extracted from the ratios

$$\mathcal{R}^{\pm}_{4ij} = \frac{C^{\pm}_{4ij}(t, \boldsymbol{p})}{C_4(t, \boldsymbol{p})} = -p_i p_j R^{\pm}, \tag{17}$$

where $\langle \xi^2 \rangle^{\text{bare}} = R^-$ and $a_2^{\text{bare}} = \frac{7}{12}(5R^- - R^+)$. In our calculations we use the interpolator $J = \mathcal{P}$, as this gives a better overlap with the ground state than $\mathcal{A}_4$.

The renormalized moments in the $\overline{\text{MS}}$ scheme read

$$\langle \xi^2 \rangle^{\overline{\text{MS}}} = \zeta_{11} R^- + \zeta_{12} R^+, \tag{18}$$

$$a_2^{\overline{\text{MS}}} = \frac{7}{12}\left[5\zeta_{11} R^- + (5\zeta_{12} - \zeta_{22}) R^+\right], \tag{19}$$

where ζ_{ij} are ratios of renormalization constants which are defined in Ref. [12].

2.3. Momentum smearing

On a lattice of $N_s^3 N_t$ sites, separated by the lattice constant a, the linear spatial extent is given as $L = N_s a$ and spatial momentum components are quantized in terms of integer multiples of $2\pi/L$. The calculation of the second moment of the DA requires a spatial momentum $\boldsymbol{p} = (2\pi/L)\boldsymbol{n_p}$, with at least two non-vanishing components, i.e., $\boldsymbol{n_p}^2 \geq 2$. This, in addition to employing two derivatives, considerably deteriorates the signal-to-noise ratio. This problem is ameliorated by using momentum smearing [6]. Here we briefly summarize this method.

It is well known that spatially smearing the quark creation and destruction operators used within the construction of hadronic interpolating fields increases the overlap of the generated superposition of hadronic states with the ground state within a given channel. This is not surprising, as ground state hadrons have smooth, spatially extended wave functions. The smearing operator F should be self-adjoint, gauge covariant and a singlet with respect to all global transformations that act on a timeslice. In the non-interacting case its action on a quark field q can be expressed as a convolution with a scalar kernel function f:

$$(Fq)_{\boldsymbol{x}} = \sum_{\boldsymbol{y}} f(\boldsymbol{x} - \boldsymbol{y}) q_{\boldsymbol{y}}. \tag{20}$$

In momentum space this convolution becomes a product.

If our smearing kernel is a real Gaussian, then in momentum space it will remain a Gaussian centred around $\boldsymbol{k} = \boldsymbol{0}$. If the hadron carries a non-vanishing momentum $\boldsymbol{p}$, it is natural to assume that the quark will carry a momentum fraction $\boldsymbol{k} = \zeta \boldsymbol{p}$. We remark that there is no obvious relation between ζ and the longitudinal momentum fraction x of the light-cone wave function. A Gaussian wave function with width σ that is centred about the momentum $\boldsymbol{k}$ acquires a phase:

$$f_{(\boldsymbol{k})}(\boldsymbol{x} - \boldsymbol{y}) = f_{(\boldsymbol{0})}(\boldsymbol{0}) \exp\left[-\frac{(\boldsymbol{x} - \boldsymbol{y})^2}{2\sigma^2} + i\boldsymbol{k}(\boldsymbol{x} - \boldsymbol{y})\right], \tag{21}$$

where $f_{(\boldsymbol{0})} = f$. Our periodic lattice appears to imply a quantization of the possible values of $\boldsymbol{k}$. However, Eq. (21) can also be cast into an iterative process, lifting this limitation: It is well known that in infinite volume the above convolution $F_{(\boldsymbol{k})}q$ can be obtained as the result of evolving the heat equation with a drift term,

$$\frac{\partial q(\tau)}{\partial \tau} = \alpha(\nabla - i\boldsymbol{k})^2 q(\tau), \tag{22}$$

starting from a spatial delta source at $\tau = 0$, to the fictitious time $\tau = \sigma^2/(2\alpha)$.

Table 1
List of the ensembles used in this work. $\beta = 3.4$ corresponds to the lattice spacing $a \approx 0.0857$ fm and N_c denotes the number of analysed configurations. A detailed description of these ensembles can be found in Refs. [15,20].

id	N_s	N_t	m_π [MeV]	m_K [MeV]	$m_\pi L$	N_c
H101	32	96	420	420	5.8	2000
H102	32	96	355	440	4.9	1997
H105	32	96	280	465	3.9	2833
C101	48	96	222	474	4.6	1552

One can approximate Eq. (22) by a discrete process, defining $F_{(\boldsymbol{k})} = \Phi^n_{(\boldsymbol{k})}$ as the nth application of an elementary iteration,

$$(\Phi_{(\boldsymbol{k})} q)_{\boldsymbol{x}} = \frac{1}{1 + 6\varepsilon}\left[q_{\boldsymbol{x}} + \varepsilon \sum_{j=\pm 1}^{\pm 3} U_{\boldsymbol{x},j} e^{-i\boldsymbol{k}\hat{\boldsymbol{\jmath}}} q_{\boldsymbol{x}+\hat{\boldsymbol{\jmath}}}\right], \tag{23}$$

where $U_{\boldsymbol{x},j}$ is the gauge link connecting the lattice points $\boldsymbol{x}$ and $\boldsymbol{x} + \hat{\boldsymbol{\jmath}}$, for details see Refs. [6,15]. In practice this smearing is implemented by multiplying the spatial connectors within the timeslice in question by the appropriate phases, $U_{\boldsymbol{x},j} \mapsto e^{-iak_j} U_{\boldsymbol{x},j}$. For $\boldsymbol{k} = \boldsymbol{0}$ Eq. (23) corresponds to the well-known Wuppertal smearing [16,17]. The time coordinate is suppressed as the smearing is local in time.

The gauge connectors within Eq. (23), $U_{\boldsymbol{x},j}$ and $U_{\boldsymbol{x},-j} \equiv U^{\dagger}_{\boldsymbol{x}-\hat{\boldsymbol{\jmath}},j}$, where $\hat{\boldsymbol{\jmath}}$ denotes a vector of length a and direction j, are spatially APE smeared [18]:

$$U^{(m+1)}_{\boldsymbol{x},i} = \mathcal{P}_{\text{SU(3)}}\left(\delta\, U^{(m)}_{\boldsymbol{x},i} + \sum_{|j|\neq i} U^{(m)}_{\boldsymbol{x},i} U^{(m)}_{\boldsymbol{x}+\hat{\boldsymbol{\jmath}},i} U^{(m)\dagger}_{\boldsymbol{x}+\hat{\boldsymbol{\imath}},j}\right), \tag{24}$$

where $i \in \{1, 2, 3\}$ and $j \in \{\pm 1, \pm 2, \pm 3\}$. The sum is over the four spatial "staples" surrounding $U_{\boldsymbol{x},i}$, and $\mathcal{P}_{\text{SU(3)}}$ is a gauge covariant projector onto the gauge group SU(3), defined by maximizing $\text{Re}\,\text{Tr}\{A^{\dagger}\mathcal{P}_{\text{SU(3)}}(A)\}$. If the APE smeared links are close to unit fields then the width parameter of the resulting Gaussian is given as [6][1]

$$\sigma \approx \sqrt{2na^2}\sqrt{\frac{\varepsilon}{1 + 6\varepsilon}}, \tag{25}$$

where large values of ε will allow for smaller iteration counts n, but the resulting function will be less smooth.

In the meson case the quark creation operator at the source needs to be smeared with $F_{(\boldsymbol{k})}$ and the quark destruction operator with $F_{(-\boldsymbol{k})}$, while for baryons all three quarks should be smeared with $F_{(\boldsymbol{k})}$, see Ref. [6] for details.[2]

3. Results

We illustrate the reduction of statistical errors of the two-point functions that enter the calculation of the second moment of the pion DA, using the momentum smearing technique. For this purpose we consider four Coordinated Lattice Simulations (CLS) ensembles, listed in Table 1. These ensembles were generated using the lattice action defined in Ref. [15] and employing open boundary conditions for the gauge fields in the temporal direction. They

[1] The root mean squared width of the resulting Gaussian will correspond to $\sqrt{3}\sigma$ as we have three spatial dimensions. This will shrink by a factor $1/\sqrt{2}$ if we consider the squared wave function and since we will smear both quark and antiquark, the pion interpolator will be wider by a factor $\sqrt{2}$ than the individual quark fields.

[2] The sign of the complex phase in Eqs. (21), (22) and (23) is opposite to that of Ref. [6]. Here we assume that the phase of the momentum projection at the sink reads $e^{-i\boldsymbol{px}}$ and $\boldsymbol{k} = \zeta \boldsymbol{p}$ with $\zeta \geq 0$. The phase used in Ref. [6] corresponds to the non-standard $e^{+i\boldsymbol{px}}$ convention that is used within the CHROMA software suite [19].

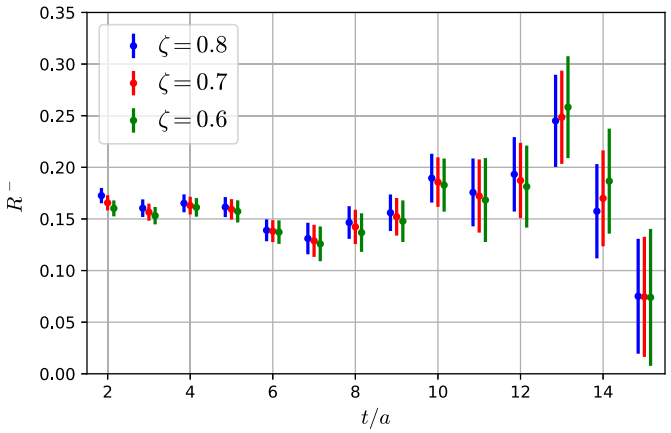

Fig. 1. Comparison of different values for the parameter ζ, using the bare lattice value of R^- (see Eq. (17)) at the squared momentum $\boldsymbol{p}^2 = 2(2\pi/L)^2 \approx (0.64\ \mathrm{GeV})^2$ obtained from 331 configurations of the ensemble H105. (For interpretation of the references to colour in this figure legend, the reader is referred to the web version of this article.)

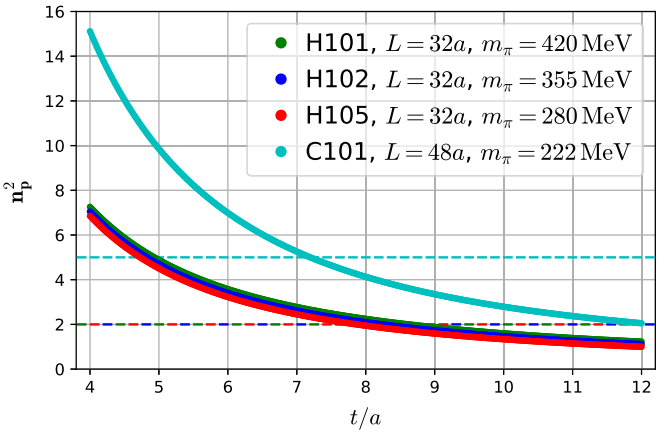

Fig. 2. The optimal $\boldsymbol{n}_{\boldsymbol{p}}^2$, according to the model Eq. (28), as a function of t/a for each ensemble. (For interpretation of the references to colour in this figure legend, the reader is referred to the web version of this article.)

comprise between $N_c \approx 1500$ to $N_c \approx 2800$ configurations, separated by four hybrid Monte Carlo molecular dynamics units. The statistical errors were evaluated using the Bootstrap procedure, with $N_{\mathrm{samples}} = 500$, combined with the binning method, where blocks of N_{bin} consecutive configurations are used. We have observed that a binsize of $N_{\mathrm{bin}} = 10$ saturates the statistical error.

The gauge links entering the quark smearing were APE smeared according to Eq. (24), employing 25 iterations with the parameter $\delta = 2.5$. We applied both, the standard Wuppertal smearing [16,17] and the novel momentum smearing, i.e., we implemented Eq. (23) setting $\boldsymbol{k} = \boldsymbol{0}$ and $\boldsymbol{k} \neq \boldsymbol{0}$, respectively, and applied 300 smearing steps with the smearing parameter $\varepsilon = 0.25$. The root mean squared width of the squared pion interpolator wave function can be estimated using Eq. (25). This gives $\sqrt{3}\sigma \approx \sqrt{3} \cdot 0.664$ fm $\approx$ 1.14 fm.

After studying the improvement achieved through momentum smearing, we attempt a chiral extrapolation of our results at a fixed lattice spacing $a \approx 0.0857$ fm.

3.1. Optimizing the smearing and the momentum

In order to obtain the second moment of the pion DA we compute ratios of two-point functions that are smeared at the source and local at the sink (smeared-point), where the physical momenta $\boldsymbol{p}$ and smearing vectors $\boldsymbol{k}$ are parallel:

$$\boldsymbol{k} = \zeta\, \boldsymbol{p}. \tag{26}$$

One may naively expect that a value $\zeta \lesssim 1/2$ was optimal, evenly distributing the meson momentum between quark and antiquark, however, Ref. [6] indicated that a value $\zeta \approx 0.8$ was preferable. We confirm that by decreasing ζ from 0.8 to 0.6, no discernable improvement of the ground state overlap can be observed, see Fig. 1 for the example of the ratio R^-. If at all, the statistical errors become slightly larger. In the following we therefore stick to the suggested value of $\zeta = 0.8$.

Using the momentum smearing for mesons, one needs two inversions per momentum vector $\boldsymbol{n_p}$. In contrast to baryonic two-point functions, where all quarks propagate in the forward direction and therefore are smeared using $f_{(\boldsymbol{k})}$, the antiquark in mesonic two-point functions needs to be smeared with $f_{(-\boldsymbol{k})}$.

It is instructive to determine which momentum vector $\boldsymbol{n_p}$ produces the best signal for a given ensemble. We make a crude approximation for the signal-to-noise ratio $S(t)$ by assuming a time-independent noise function. Then the signal-to-noise ratio of the numerator (which dominates the error of the combination Eq. (17)) can be estimated as

$$S(t) \propto p_i p_j \exp\bigl(-\sqrt{m_\pi^2 + \boldsymbol{p}^2} t\bigr). \tag{27}$$

Maximizing this expression with respect to $\boldsymbol{p}^2$ gives the positive solution

$$\boldsymbol{p}^2 = \frac{2}{t^2}\bigl(1 + \sqrt{1 + m_\pi^2 t^2}\bigr). \tag{28}$$

Clearly, the optimal choice of momentum for a given correlation function depends on t and lower momenta will always be preferred at large values of t. This means the outcome will depend on the fit window in t and this in turn will depend on the available statistics. To aid in finding the most appropriate momentum, we plot Eq. (28) in Fig. 2 for the typical fit range for our different ensembles, $t = 4a$–$12a$. Based on this model, we can read off that for the $L = 32a$ lattices squared momenta in the vicinity of $\boldsymbol{n}_{\boldsymbol{p}}^2 = 2$ should give reasonable results, whereas for the larger $L = 48a$ lattice values of $\boldsymbol{n}_{\boldsymbol{p}}^2$ closer to 5 should be investigated. As an example, in Fig. 3 we show the results of the bare observables $R^\pm$ calculated for different momenta $\boldsymbol{p}$ on the $L = 48a$ C101 ensemble. For small values of t/a, larger $\boldsymbol{p}^2$ exhibit smaller statistical errors, whereas for large values of t/a, the error increases with $\boldsymbol{p}^2$. Thus there is a window for an optimal choice of momentum.

In our further analysis we choose $\boldsymbol{n_p} = (1,1,0)$, $\boldsymbol{n_p} = (1,0,1)$ and $\boldsymbol{n_p} = (0,1,1)$ for the ensembles with a spatial extent of $L = 32a$ and $\boldsymbol{n_p} = (2,1,0)$, $\boldsymbol{n_p} = (2,0,1)$ and $\boldsymbol{n_p} = (0,2,1)$ for the C101 ensemble. For the $L = 32a$ lattices we employ a single source position, while for C101 we realize on average 2 source positions on each configuration.

3.2. Momentum smearing versus Wuppertal smearing

Fig. 4 shows the plateau of R^+ (left) and R^- (right) for the H105 lattice with $N_c = 2830$ for both smearing methods. Clearly the momentum smearing generates a much cleaner and longer plateau with very small statistical errors. In contrast to the standard Wuppertal smearing, where errors increase rapidly for high values of t, the signal-to-noise problem is less severe for the momentum smearing. Moreover, in some cases, such as R^+ (shown in Fig. 4), we notice reduced contaminations from excited states.

In Fig. 4 we compared the results for the same number of configurations. However, the novel momentum smearing method is computationally more expensive. In general one can average

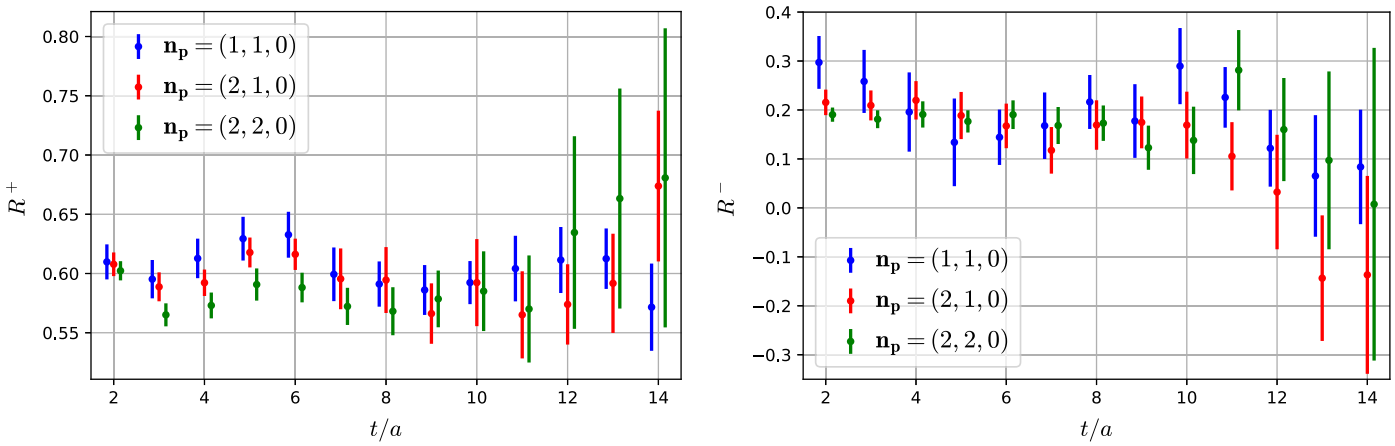

Fig. 3. Value of $R^{\pm}$ for C101 ($m_\pi = 222$ MeV) with different momenta $\boldsymbol{p}$ using 52 configurations. (For interpretation of the references to colour in this figure legend, the reader is referred to the web version of this article.)

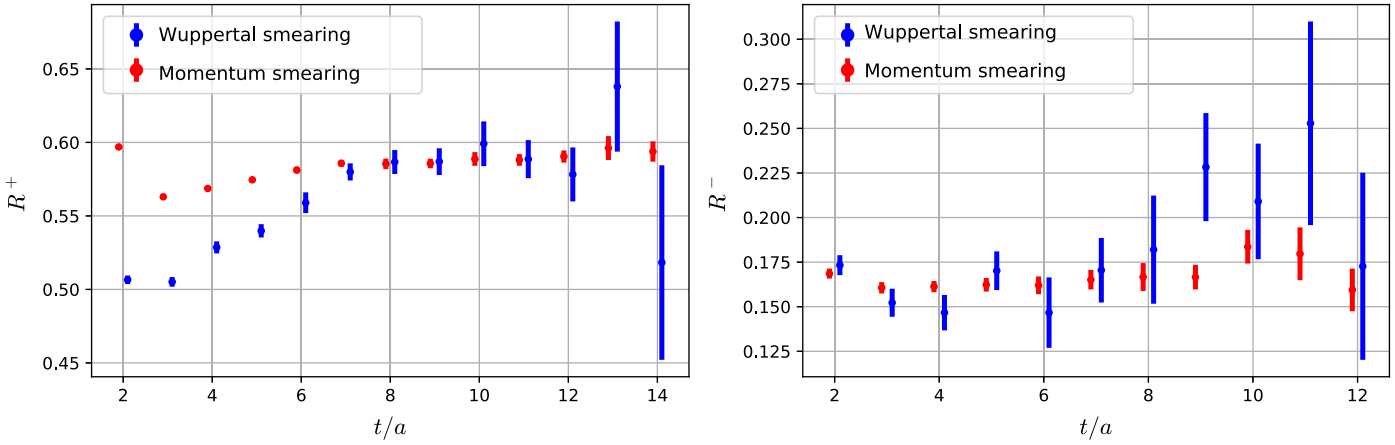

Fig. 4. Comparison of the bare lattice values of R^- for H105 ($m_\pi = 280$ MeV) using the standard Wuppertal smearing and the new momentum smearing techniques. (For interpretation of the references to colour in this figure legend, the reader is referred to the web version of this article.)

Table 2
Equal cost comparison of the errors obtained with both methods on the H105 lattice for $R^{\pm}$. We show the squared ratio of the statistical errors of Wuppertal smearing over momentum smearing divided by the number of inversions needed for each method.

t/a	3	4	5	6	7	8	9	10	11	12
R^-	1.01	1.64	1.35	2.60	1.82	2.51	3.20	1.96	2.48	3.21
R^+	0.85	0.97	1.03	1.64	1.03	0.85	1.28	1.76	1.77	3.24

over momenta that are equivalent in terms of the cubic symmetry group O_h. Taking into account that the results for $\boldsymbol{p}$ and $-\boldsymbol{p}$ are trivially related, this gives, depending on the momentum, up to 12 possible lattice directions. For the Wuppertal smearing, additional momenta are computationally almost for free, as they only require additional Fourier sums. In contrast, for the momentum smearing each momentum direction requires new, differently smeared sources. For the pion two inversions, with momenta $\boldsymbol{k}$ and $-\boldsymbol{k}$, are necessary as discussed in Sec. 2.3. For $\boldsymbol{n}_{\boldsymbol{p}}^2 = 2$ this means that momentum smearing is by a factor of almost 6 more expensive than Wuppertal smearing. Therefore, in Table 2 we provide an equal cost comparison of the ratios of errors obtained using both methods for the H105 lattice. Even at equal cost, we still see a reduction of the squared error by up to a factor 3, in particular for the physically more relevant R^- ratio. Note that for R^+, this factor is around 1 for small t/a, but grows after the ground state plateau is reached for $t > 7a$. The reduction in error is not only a local effect on individual timeslices, it persist also when performing a fully correlated fit in the plateau region. Note that for mesons containing non-degenerate quarks, the traditional method becomes more expensive as this will also require two inversions, while for baryon interpolators no momentum smearing with $-\boldsymbol{k}$ is required. This means that in terms of a real cost comparison the pion is the least favourable case for momentum smearing.

For a fixed number of measurements the gain of momentum smearing is even larger than at a fixed computational cost. However, the reduction of errors that can be achieved by increasing the number of measurements on each configuration is limited, as additional measurements will become increasingly correlated.

3.3. Chiral extrapolation

We use Chiral Perturbation Theory (ChPT) to extrapolate the results obtained with the new momentum smearing to physical quark masses. The CLS lattice ensembles used in this work are chosen such that they lie on the $\mathrm{Tr}\, M = \text{const.}$ line [15,20], which means that to next-to-leading order SU(3) ChPT the average quadratic meson mass,

$$2m_K^2 + m_\pi^2, \tag{29}$$

is kept fixed at its physical value, up to lattice spacing effects. Thus the extrapolation $m_\pi \to m_\pi^{\mathrm{phys}}$ also corresponds to $m_K \to m_K^{\mathrm{phys}}$.

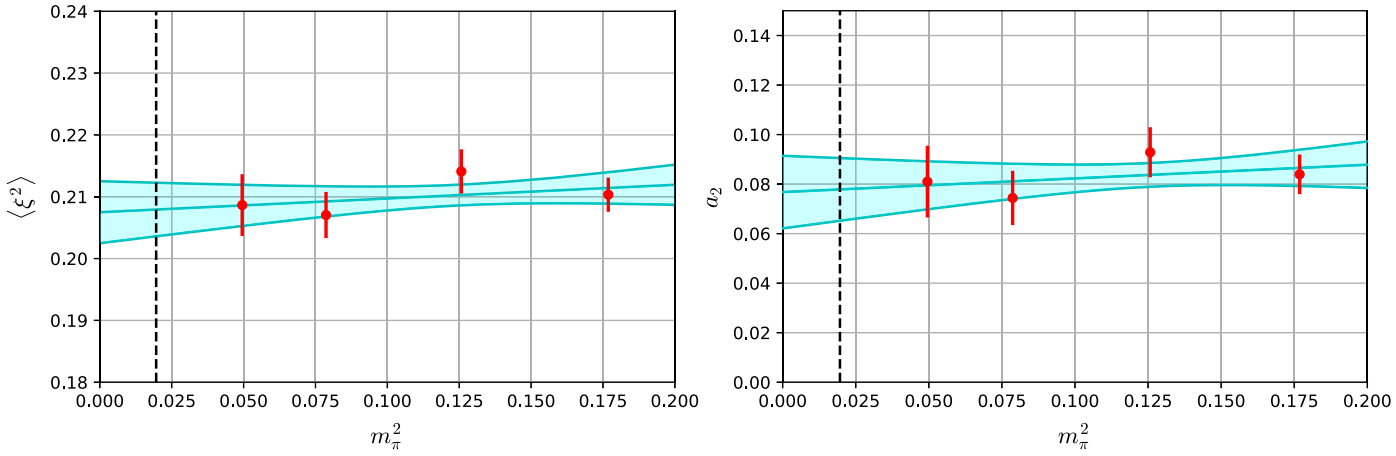

Fig. 5. Mean and one standard deviation error bands of the chiral extrapolation of $\langle \xi^2 \rangle$ (left) and a_2 (right). The vertical dotted line indicates the physical pion mass.

Up to one-loop order, $\langle \xi^2 \rangle^{\overline{\rm MS}}$ and $a_2^{\overline{\rm MS}}$ do not contain chiral logarithms [21], and we assume a linear behaviour in m_π^2,

$$\langle \xi^2 \rangle = \langle \xi^2 \rangle^{(0)} + \langle \xi^2 \rangle^{(2)} m_\pi^2, \tag{30}$$

$$a_2 = a_2^{(0)} + a_2^{(2)} m_\pi^2, \tag{31}$$

where $\langle \xi^2 \rangle^{(n)}$ are LECs of the fit. The chiral extrapolation is depicted in Fig. 5. At the physical point we find

$$\langle \xi^2 \rangle^{\overline{\rm MS}}(2\ {\rm GeV}) = 0.2077(43), \tag{32}$$

$$a_2^{\overline{\rm MS}}(2\ {\rm GeV}) = 0.0762(127). \tag{33}$$

We remark that these numbers were obtained at the fixed lattice spacing $a \approx 0.0857$ fm and no continuum limit has been performed yet. Since the goal of this study was not to obtain a new measurement for the second moment but to compare the two smearing methods, we give no error estimates aside from the statistical one and also refrain from comparing our values to other results in the literature. These topics shall be addressed in a future work, where we will explore a rich landscape of CLS ensembles to obtain a new high precision result including a detailed error analysis and comparison.

4. Summary

In this work we have illustrated the effectiveness and advantages of the novel momentum smearing method compared to the standard Wuppertal smearing. For the special case of the pion the momentum smearing requires more inversions, relative to Wuppertal smearing, than for baryons or for mesons consisting of mass non-degenerate quarks. Nevertheless, we have still obtained smaller errors at a similar computational effort. Clearly, using the momentum smearing technique on a fixed number of available configurations, much smaller statistical errors can be achieved. Since for each momentum a new inversion is required in any case, one may suspect that combining the momentum smearing method with the stochastic one-end-trick [22] even bigger gains can be achieved. We have not investigated this possibility as yet.

In future studies the momentum smearing will be applied to mesons and baryons on additional CLS lattices, including ensembles at (nearly) physical quark masses and various lattice spacings down to $a \approx 0.04$ fm. This will expand our previous work on meson and baryon DAs [12,13] and enable us to perform systematic continuum limit extrapolations for mesons and octet baryons.

Acknowledgements

This work has been supported by the Deutsche Forschungsgemeinschaft (SFB/TRR-55) and the Studienstiftung des deutschen Volkes. A significant part of the analysis was carried out on the QPACE 2 [23] Xeon Phi installation of the SFB/TRR-55 in Regensburg. Additional computations were performed on computers of various institutions which we acknowledge below. The ensembles were generated using openQCD [24]. We used a modified version of the Chroma [19] software package along with the LibHadronAnalysis library and the multigrid solver implementation of Ref. [25] (see also Ref. [26]) to generate hadronic two-point functions. We thank Benjamin Gläßle and Daniel Richtmann for code development, discussions and software support. Last but not least we thank all our CLS colleagues.

The authors gratefully acknowledge the Interdisciplinary Centre for Mathematical and Computational Modelling (ICM) of the University of Warsaw for computer time on Okeanos (grant No. GA67-12). We also acknowledge the Gauss Centre for Supercomputing (GCS) for providing computing time for a GCS Large-Scale Project on the GCS share of the supercomputer SuperMUC at Leibniz Supercomputing Centre (LRZ, www.lrz.de). GCS is the alliance of the three national supercomputing centres HLRS (Universität Stuttgart), JSC (Forschungszentrum Jülich), and LRZ (Bayerische Akademie der Wissenschaften), funded by the German Federal Ministry of Education and Research (BMBF) and the German State Ministries for Research of Baden-Württemberg (MWK), Bayern (StMWFK) and Nordrhein-Westfalen (MIWF).

References

[1] J. Dudek, et al., Physics opportunities with the 12 GeV upgrade at Jefferson Lab, Eur. Phys. J. A 48 (2012) 187, arXiv:1208.1244 [hep-ex].
[2] D. Boer, et al., Gluons and the quark sea at high energies: distributions, polarization, tomography, arXiv:1108.1713 [nucl-th].
[3] Belle II Collaboration, T. Abe, et al., Belle II Technical Design Report, arXiv:1011.0352 [physics.ins-det].
[4] V.M. Braun, D. Müller, Exclusive processes in position space and the pion distribution amplitude, Eur. Phys. J. C 55 (2008) 349, arXiv:0709.1348 [hep-ph].
[5] X. Ji, Parton physics on a Euclidean lattice, Phys. Rev. Lett. 110 (2013) 262002, arXiv:1305.1539 [hep-ph].
[6] RQCD Collaboration, G.S. Bali, B. Lang, B.U. Musch, A. Schäfer, Novel quark smearing for hadrons with high momenta in lattice QCD, Phys. Rev. D 93 (2016) 094515, arXiv:1602.05525 [hep-lat].
[7] C. Alexandrou, K. Cichy, M. Constantinou, K. Hadjiyiannakou, K. Jansen, F. Steffens, C. Wiese, Parton distributions from lattice QCD with momentum smearing, PoS LATTICE2016 (2016) 151, arXiv:1612.08728 [hep-lat].
[8] G. Martinelli, C.T. Sachrajda, A lattice calculation of the second moment of the pion's distribution amplitude, Phys. Lett. B 190 (1987) 151.

[9] QCDSF and UKQCD Collaborations, V.M. Braun, et al., Moments of pseudoscalar meson distribution amplitudes from the lattice, Phys. Rev. D 74 (2006) 074501, arXiv:hep-lat/0606012.
[10] RBC and UKQCD Collaborations, R. Arthur, P.A. Boyle, D. Brömmel, M.A. Donnellan, J.M. Flynn, A. Jüttner, T.D. Rae, C.T.C. Sachrajda, Lattice results for low moments of light meson distribution amplitudes, Phys. Rev. D 83 (2011) 074505, arXiv:1011.5906 [hep-lat].
[11] V.M. Braun, S. Collins, B. Gläßle, M. Göckeler, A. Schäfer, R.W. Schiel, W. Söldner, A. Sternbeck, P. Wein, Light-cone distribution amplitudes of the nucleon and negative parity nucleon resonances from lattice QCD, Phys. Rev. D 89 (2014) 094511, arXiv:1403.4189 [hep-lat].
[12] V.M. Braun, S. Collins, M. Göckeler, P. Pérez-Rubio, A. Schäfer, R.W. Schiel, A. Sternbeck, Second moment of the pion light-cone distribution amplitude from lattice QCD, Phys. Rev. D 92 (2015) 014504, arXiv:1503.03656 [hep-lat].
[13] G.S. Bali, et al., Light-cone distribution amplitudes of the baryon octet, J. High Energy Phys. 02 (2016) 070, arXiv:1512.02050 [hep-lat].
[14] J.L. Rosner, S. Stone, R.S. Van de Water, Leptonic decays of charged pseudoscalar mesons – 2015, arXiv:1509.02220 [hep-ph], submitted to Particle Data Book.
[15] M. Bruno, et al., Simulation of QCD with $N_f = 2 + 1$ flavors of non-perturbatively improved Wilson fermions, J. High Energy Phys. 02 (2015) 043, arXiv:1411.3982 [hep-lat].
[16] S. Güsken, U. Löw, K.-H. Mütter, R. Sommer, A. Patel, K. Schilling, Nonsinglet axial vector couplings of the baryon octet in lattice QCD, Phys. Lett. B 227 (1989) 266.
[17] S. Güsken, A study of smearing techniques for hadron correlation functions, Nucl. Phys. B, Proc. Suppl. 17 (1990) 361.
[18] M. Falcioni, M.L. Paciello, G. Parisi, B. Taglienti, Again on SU(3) glueball mass, Nucl. Phys. B 251 (1985) 624.
[19] SciDAC, LHPC, and UKQCD Collaborations, R.G. Edwards, B. Joó, The chroma software system for lattice QCD, Nucl. Phys. B, Proc. Suppl. 140 (2005) 832, arXiv:hep-lat/0409003.
[20] RQCD Collaboration, G.S. Bali, E.E. Scholz, J. Simeth, W. Söldner, Lattice simulations with $N_f = 2 + 1$ improved Wilson fermions at a fixed strange quark mass, Phys. Rev. D 94 (2016) 074501, arXiv:1606.09039 [hep-lat].
[21] J.-W. Chen, H.-M. Tsai, K.-C. Weng, Model-independent results for SU(3) violation in twist-3 light-cone distribution functions, Phys. Rev. D 73 (2006) 054010, arXiv:hep-ph/0511036.
[22] UKQCD Collaboration, M. Foster, C. Michael, Hadrons with a heavy color-adjoint particle, Phys. Rev. D 59 (1999) 094509, arXiv:hep-lat/9811010.
[23] P. Arts, et al., QPACE 2 and domain decomposition on the Intel Xeon phi, PoS LATTICE2014 (2015) 021, arXiv:1502.04025 [cs.DC].
[24] M. Lüscher, S. Schaefer, Lattice QCD with open boundary conditions and twisted-mass reweighting, Comput. Phys. Commun. 184 (2013) 519, arXiv:1206.2809 [hep-lat].
[25] S. Heybrock, M. Rottmann, P. Georg, T. Wettig, Adaptive algebraic multigrid on SIMD architectures, PoS LATTICE2015 (2016) 036, arXiv:1512.04506 [physics.comp-ph].
[26] A. Frommer, K. Kahl, S. Krieg, B. Leder, M. Rottmann, Adaptive aggregation-based domain decomposition multigrid for the lattice Wilson–Dirac operator, SIAM J. Sci. Comput. 36 (2014), arXiv:1303.1377 [hep-lat].